Study on Numerical Analysis of Cavity Subjected to Inner Step Uniform Pressure Modeled by Boundary Element Method

Abbas Eslami Haghighat[1*] and Ramezan Ali Izadifard[2]

1. Assistant Professor, Department of Civil Engineering, Faculty of Engineering, Urmia University, Urmia, Iran, * Corresponding Author; email: a.eslami@urmia.ac.ir
2. Assistant Professor, Department of Civil engineering, Imam Khomeini University, Qazvin, Iran

Received: 11/01/2014
Accepted: 01/09/2014

ABSTRACT

In this paper, cylindrical cavities under pressure located in full space and half space are separately analyzed. Boundary element method formulated in frequency domain is used to discretize the boundary of the problems. Infinite boundary included in the problems is modeled by a special boundary named enclosing boundary. The response in the time-domain is then obtained from the frequency-domain solution using Fast Fourier Transform (FFT) technique. The proposed approach is applied to Selberg problem, which consists of a cylindrical cavity in a full space loaded normal to its wall as well as the one in a half space with the same loading condition. Comparison of the obtained results with the closed form and existing numerical solutions shows that the enclosing boundary of any shape can effectively be used to model radiation of the outgoing waves into infinity. It has also been shown that the Poisson's ratio of the medium is a predominant parameter, which can influence the response of the underground cavities.

Keywords:
Boundary element method; Underground cavity; Infinite media; Enclosing boundary; Poisson's ratio

1. Introduction

Underground structures such as subway tunnels, culverts, pipelines and oil reservoirs and their dynamic behaviors are the subject of many research projects. Different analytical and numerical methods are undertaken to compute the seismic responses of such buried structures.

Analytical methods were basically developed to consider simple geometries of the cavities, including circular, spherical or elliptical shapes in an infinite or semi-infinite media. Baron and Matthews [1] determined the displacement and stress fields around a circular cavity due to traveling P-wave. The effect of traction-free surface in dynamic response of a circular cavity subjected to SH-wave was considered by Lee and Trifunac [2]. Analytical solution for truncated circular cavity subjected to vertically propagating SH wave is obtained by Tsaur and Chang [3]. Wong et al study the response of an infinitely long buried tunnel swept by P, SV and Rayleigh waves using a semi-analytical method [4].

Finite-element method which is the most versatile computational method has been used to analyze buried structures with arbitrary geometry, complex material behavior and medium inhomogeneities. Analysis of parallel tunnels due to moving loads [5], dynamic response of buried frameworks [6] and the effect of blast loads to buried structures [7] are some examples of application of the finite finite-element method in this area. Finite difference method has also been used to study the response of underground protective structures due to surface blast [8].

The Boundary Element Method (BEM) which is a suitable tool especially for elastodynamic problems was used to obtain the response of cavity subjected to incident waves. The response of embedded cavity due to harmonic incident SH, P, SV and Rayleigh waves is obtained using indirect BEM by Benites et al [9] and Luco and de Baross [10]. Alielahi et al [11] studied the seismic ground motion due to underground circular cavity subjected to incident P and SV wave. Time-domain solutions for full and truncated embedded circular cavities subjected to vertically traveling SH wave using half-plane fundamental solution are presented by Panji et al [12]. The BEM is also applied for analyzing of tunnels of arbitrary shapes subjected to travelling waves [13]. Seismic response of tunnels considering traction-free surface was investigated by Kontoni et al [14]. Scattering of P, SV and Rayleigh waves by smooth and rough under-surface circular cavity has been obtained by Yu and Dravinski [15] using boundary integral equation method. Multiple scattering problems such as interaction between a tunnel and a triangular canyon has been solved efficiently by Shah et al [16]. Scattering of SH waves due to multiple cavities [17] or interaction between a truncated circular cavity and valley [18] are studied by some researchers. Dravinski [19] also studied the scattering of SH, SV, P and Rayleigh waves by several inclusions of arbitrary shapes. BEM has also been used to analyze the time-harmonic response of a lined semicircular tunnel in a poroelastic medium [20].

There are essentially two approaches in order to solve the above-mentioned elastodynamic problems by using the BEM. In the first one, the BEM is formulated in the time domain, and the transient response is obtained directly by solving boundary element equations using time marching method. In the second one, the boundary element method is formulated in a transformed domain, and the transient response is then obtained by inverse transform algorithm.

In this paper, the capability and efficiency of time-frequency domain direct boundary element method with dummy nodes and enclosing elements in solving elastodynamic problems are investigated. Two examples consist of cylindrical cavities in full and half spaces subjected to suddenly applied uniform interior pressure are solved for different values of Poisson's ratios as well as various depths of the cavity. Hoop stress for these problems is obtained without solving boundary integral equation for stress and corresponding complicated fundamental solutions. It is also shown that the radiation condition in infinite and semi-infinite boundaries can be modeled successfully by enclosing boundary of any arbitrary shape.

2. BE Formulation

The BE method is a powerful numerical technique for analysis of homogeneous elastic medium in the static and dynamic states. Neglecting the body forces, the governing boundary integral equation for a two dimensional homogeneous, elastic and isotropic medium can be obtained by using Betti's reciprocal theorem as follows:

$$c_{ij}(\eta)\,u_j(\eta) = -\int_L p^*_{ij}(\xi,x)\,u_j(x)\,dL(x) + \int_L p_{ij}(x)\,u^*_{ij}(\xi,x)\,dL(x) \tag{1}$$

where ξ denotes the source point and χ the observation point along the boundaries, u_j and p_j are respectively, displacements and tractions of points on the boundary in the j direction, $dL(x)$ is the incremental length along the boundary navigated counterclockwise, c_{ij} is the jump term equal to δ_{ij} for smooth boundaries, where δ_{ij} is Kronecker delta. $u^*_{ij}(\xi,\chi)$ and $p^*_{ij}(\xi,\chi)$ are time-harmonic fundamental solutions representing displacement and traction at the observation point χ in the j direction due to a unit harmonic point load applied at the source point ξ in the i direction in an infinite region. Fundamental solutions for two-dimensional time-harmonic in-plane problems are as follows [21]:

$$u^*_{ij} = \frac{1}{2\pi\rho C_S^2}\left[\psi\delta_{ij} - \chi r_{,i}\,r_{,j}\right] \tag{2}$$

$$p^*_{ij} = \frac{1}{2\pi}\left[\begin{array}{l}\left(\dfrac{C_P^2}{C_S^2}-2\right)\left(\dfrac{\partial\psi}{\partial r}-\dfrac{\partial\chi}{\partial r}-\dfrac{1}{r}\chi\right)r_{,i}\,n_j + \\ \left(\dfrac{\partial\psi}{\partial r}-\dfrac{\partial\chi}{\partial r}\right)\left(\delta_{ij}\dfrac{\partial r}{\partial n}+r_{,j}\,n_i\right) - \\ 2\dfrac{\chi}{r}\left(n_j r_{,i}-2r_{,i}r_{,j}\dfrac{\partial r}{\partial n}\right)-2\dfrac{\partial\chi}{\partial r}r_{,i}r_{,j}\dfrac{\partial r}{\partial n}\end{array}\right] \tag{3}$$

$$\psi = K_0\left(\frac{i\omega r}{C_S}\right)+\frac{C_S}{i\omega r}\left[K_1\left(\frac{i\omega r}{C_S}\right)-\frac{C_S}{C_P}K_1\left(\frac{i\omega r}{C_P}\right)\right] \quad (4)$$

$$\chi = K_2\left(\frac{i\omega r}{C_S}\right)-\frac{{C_S}^2}{{C_P}^2}K_2\left(\frac{i\omega r}{C_P}\right) \quad (5)$$

$$\frac{\partial\psi}{\partial r} = -\frac{i\omega}{C_S}K_1\left(\frac{i\omega r}{C_S}\right)+ \frac{C_S}{i\omega r}\left[-\frac{i\omega}{C_S}K_2\left(\frac{i\omega r}{C_S}\right)+\frac{C_S}{C_P}\frac{i\omega}{C_P}K_2\left(\frac{i\omega r}{C_P}\right)\right] \quad (6)$$

$$\frac{\partial\chi}{\partial r} = \frac{i\omega}{C_S}K_1\left(\frac{i\omega r}{C_S}\right)-\frac{2}{r}K_2\left(\frac{i\omega r}{C_S}\right)+ \frac{C_S^2}{C_P^2}\frac{i\omega}{C_P}K_1\left(\frac{i\omega}{C_P}\right)+\frac{2}{r}\frac{C_S^2}{C_P^2}K_2\left(\frac{i\omega r}{C_P}\right) \quad (7)$$

where ρ is the mass density; K_0, K_1 and K_2 are the modified Bessel functions of second kind and order zero, one and two, respectively; r is the distance between the source and the observation points; and ω, C_S and C_P are the frequency and propagation velocity of shear and pressure waves, respectively.

The boundary integral equation can be determined by discretization of the boundary into elements by proper selection of nodes. Here, isoparametric three-noded element known as quadratic element is adopted. The convoluted form of Eq. (1) is then written for every boundary points as follows:

$$\left[c_q\right]\begin{Bmatrix}u_{2q-1}\\u_{2q}\end{Bmatrix}+\sum_{e=1}^{ne}\left\{\int_{L_e}[p^*][N]dL_e\right\}\{u^e\}= \sum_{e=1}^{ne}\left\{\int_{L_e}[u^*][N]dL_e\right\}\{p^e\} \quad (8)$$

where q is the node number, ne is the number of linear boundary elements, L_e is the length of the e^{th} element, $[N]$ is the interpolation matrix and $[c_q]$ is the jump term matrix of node number q. The column vectors $\{u^e\}$ and $\{p^e\}$, represent the nodal displacement and traction vectors, respectively.

The integral over each element is carried out in the local coordinate system using standard Gauss quadrature technique. Successive application of Eq. (8) to points at the boundary results in a system of linear algebraic equations of the following form:

$$[F]\{u\} = [G]\{p\} \quad (9)$$

where $[F]$ and $[G]$ are the influence coefficients matrices and the vectors $\{u\}$ and $\{p\}$ contain the nodal displacements and tractions of all boundary nodes, respectively. After rearranging the known and unknown displacements and tractions in Eq. (9), the resulted matrix equation can be easily solved for unknown displacements and tractions at the boundary.

Having obtained all the nodal displacements and tractions of the boundary, the displacement of any interior point can be easily obtained using the convoluted form of Eq. (1) just by setting $c_{ij} = \delta_{ij}$. In order to obtain the stress components of an interior point, more complicated forms of displacement and traction fundamental solutions are required. However, the stress tensor components of the boundary points in local coordinate as shown in Figure (1) can be computed by the following expressions [22]:

$$\hat{\sigma}_{11} = \frac{1}{1-\upsilon}\left(\upsilon\hat{\sigma}_{22}+2\mu\hat{\varepsilon}_{11}\right) \quad (10)$$

$$\hat{\sigma}_{12} = \hat{p}_1 \quad (11)$$

$$\hat{\sigma}_{22} = \hat{p}_2 \quad (12)$$

where $\hat{p}_1$ and $\hat{p}_2$ are the components of the traction in local coordinates, υ denotes the Poisson's ratio and $\hat{\varepsilon}_{11}$ is the normal strain along the boundary, which can be approximated using boundary nodal displacements. Note that subscripts 1 and 2 imply the tangential and normal directions to the boundary at each point, respectively.

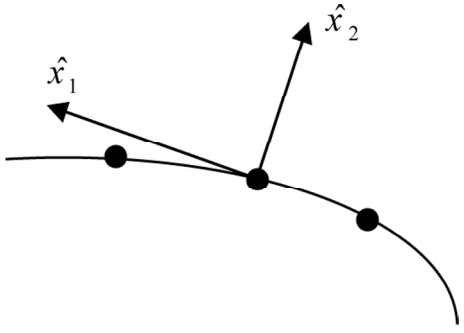

Figure 1. Local coordinate system at each point on the boundary

3. Application of the Technique

Based on the procedures outlined in the previous sections, a computer code was developed. In order to accurately compute the jump terms and corresponding diagonal terms of the matrix [*F*] in Eq. (9), enclosing elements introduced by Ahmad and Banerjee, [23], were employed to represent the infinitely extending boundaries. Enclosing boundary has been used by other researchers for diffraction of SH waves [24], as well as P and SV waves, [25]. Transient response of a medium with linear elastic behavior can be easily determined from the frequency-domain solution using FFT algorithm.

4. Numerical Examples

4.1. Pressure in the Cylindrical Cavity Located in the Full Space (Selberg Problem)

To test the credibility of the outlined procedure and verify the prepared code, the response of a cylindrical cavity of radius *R* in a full space with constant pressure *p* normal to its wall; known as Selberg problem, is considered, Figure (2). As shown in this figure, a uniform pressure is suddenly applied at time $t = 0$ and is remained constant versus time.

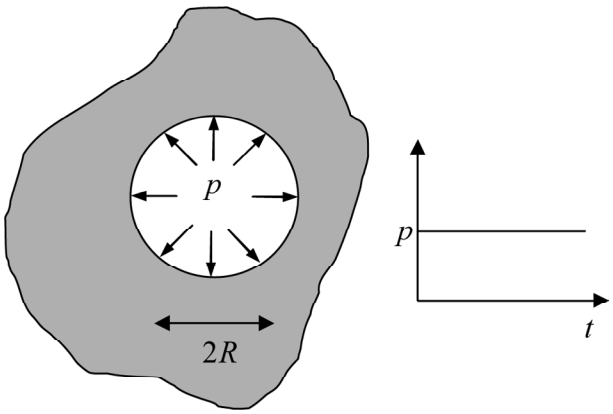

Figure 2. Geometry and loading condition of Selberg problem.

The geometry of the model is shown in Figure (3). Due to the symmetry of the loading and geometry, the boundary of the enclosing elements has a circular shape of radius 10 *R*, as first estimation. Different types of enclosing boundary of arbitrary shapes are also shown in Figure (3). It was examined that the shape of the enclosing boundary and the distance of its elements to the cavity cannot influence the obtained results. Therefore, in order to model the infinitely extending boundary, it is just enough to enclose the cavity by the enclosing boundary.

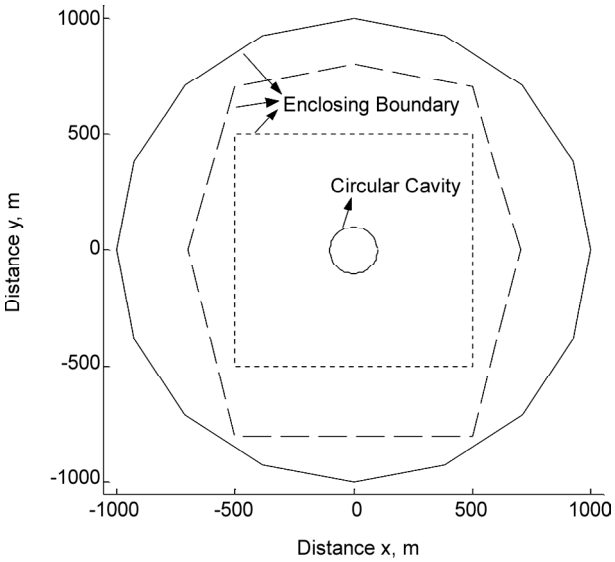

Figure 3. Different shapes of the enclosing boundaries around the circular cavity.

For boundary element analysis in the frequency domain, boundary of the region was discretized into 40 quadratic elements by 80 nodes, of which 16 nodes and corresponding eight elements are located on the enclosing boundary. The calculated frequencies are 600 in total, ranging from 0 to 1000 Hz. Maximum frequency determined the time step used in FFT algorithm.

The radial displacement of a point on the surface of the cylindrical cavity normalized by static value versus non-dimensional time, $\frac{C_p t}{R}$ is shown in Figure (4). There is a good agreement between the

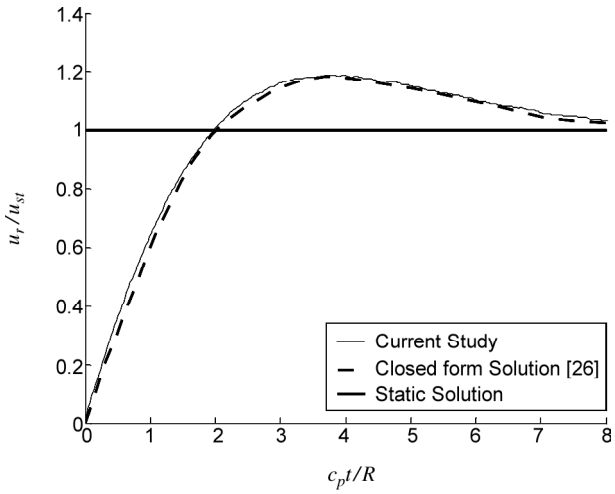

Figure 4. Normalized radial displacement versus non-dimensional time.

obtained results and the closed-form solution [26]. As expected, the response converged to the static solution for a large amount of time. Note that the results in Figure (4) correspond to Poisson's ratio of 0.2.

Variation of tangential stress, $\sigma_{\theta\theta}$, of a point on the surface boundary of the cavity known as hoop stress is then computed by Eq. (10). Figure (5) shows the hoop stress normalized by the absolute value of the interior pressure versus non-dimensional time. It should be noted that the tension stress is considered positive. Therefore, this figure shows that the amount of the static hoop stress is equal to the absolute value of the interior pressure, but it is always in tension. However, for the case in hand, the hoop stress is initially negative and its value is equal to $k_0 p$ where k_0 is the static lateral earth pressure that can be expressed in terms of Poisson's ratio. Then, in continue it changes from pressure to tension and becomes positive. Finally, it converges to the static solution as the non-dimensional time becomes larger and larger. Figure (5) also shows that the static solution of the hoop stress is independent of the Poisson's ratio of the medium.

The responses of the radial displacement and hoop stress versus non-dimensional time depicted in Figures (4) and (5) have similar patterns. There is a closed-form solution between the above-mentioned hoop stress and the radial displacement that can be expressed as follows [27]:

$$\frac{\sigma_{\theta\theta}}{p} = -1 + \frac{1}{1-\upsilon}\left(1 - 2\frac{\mu u_r}{pR}\right) \qquad (13)$$

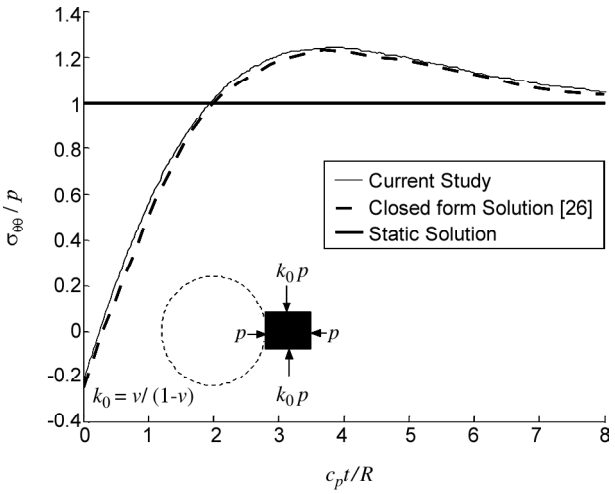

Figure 5. Normalized hoop stress versus non-dimensional time.

Using this equation, the hoop stress and radial displacement can be converted to each other. Note that the diagram of closed-form solution in Figure (4) is obtained from closed-form solution of hoop stress utilizing Eq. (13).

Figures (6) and (7) compare the time history of the radial displacement and hoop stress of a boundary point obtained by the time-frequency domain method for Poisson's ratios of 0.2, $\frac{1}{3}$ and 0.45. These values correspond to stiff, medium and soft soils, respectively. For larger values of Poisson's ratio, more amounts of time are required for convergence to the static solution, but the values of the radial displacement and hoop stress may be lower or greater depending on non-dimensional time.

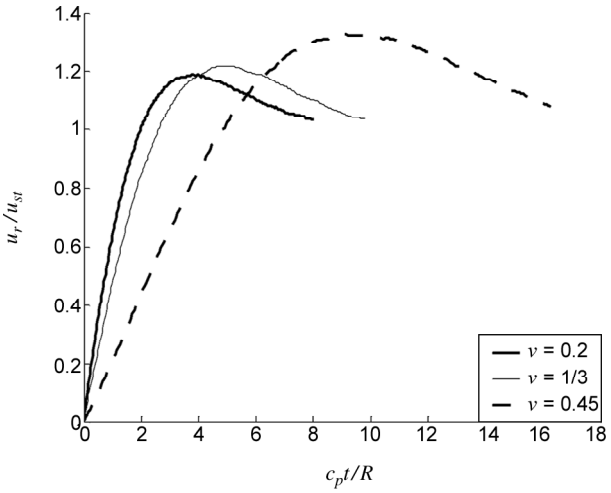

Figure 6. Normalized radial displacement of a surface point with different Poisson's ratios.

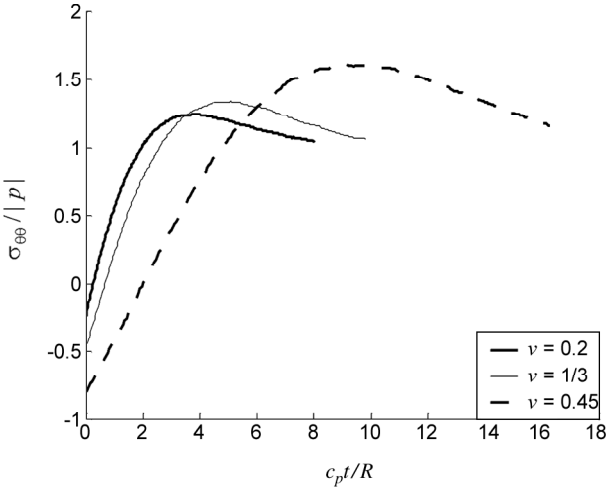

Figure 7. Normalized hoop stress of a surface point with different Poisson's ratios.

4.2. Pressure in the Underground Cylindrical Cavity

The second problem as shown in Figure (8) involves a cylindrical cavity of radius $R = 6.35$ mm located in the half space with depth $D = 2\ R$. The cavity is loaded normal to its surface at instance $t = 0$ with uniform pressure $p = 6900$ Pa. The step uniform load lasting for $15\,\mu s$. However, the observation time extends to $30\,\mu s$. The half space has the following properties: $E = 2.07 \times 10^{11}\ pa$, $\upsilon = 1/3$, $\rho = 8480\ kg/m^3$.

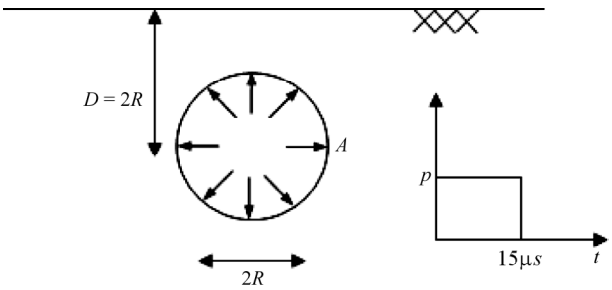

Figure 8. Geometry and loading condition of circular cavity in the half space.

The Analysis has been carried out using 86 quadratic elements and 174 nodes. 32, 50 and 4 elements are on cavity surface, traction-free surface and enclosing elements, respectively. Figure (9) shows the dimensions and different boundaries of the model. In order to properly define the corners and traction discontinuities, some dummy nodes have to be introduced in the model; two nodes are defined at one point. For this problem, two dummy nodes have to be defined at points B and C as shown in Figure (9). The calculated frequencies are 800 in total, ranging from 0 Hz to 4537205 Hz. It is worth pointing out that the static solution is also required to properly perform the FFT calculation. To do such analysis, static displacement and traction fundamental solutions are employed in a new code program.

Transient response of hoop stress of the point A at the right side of the cylindrical cavity is shown in Figure (10) and is compared with the half plane BEM [28]. Due to the multiple scattering of the generated waves between the cylindrical cavity and the traction-free surface, fluctuations in different parts of the hoop stress diagram are observed. Note that the time corresponding to point PP, is the arrival time of P wave, which emanated from the top point

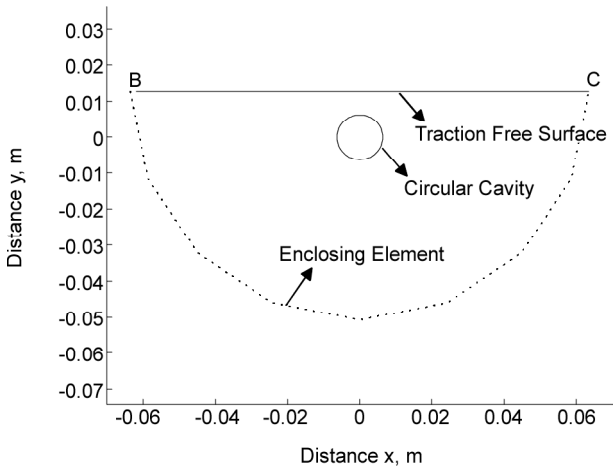

Figure 9. Model of the cavity in the half-space and different boundaries.

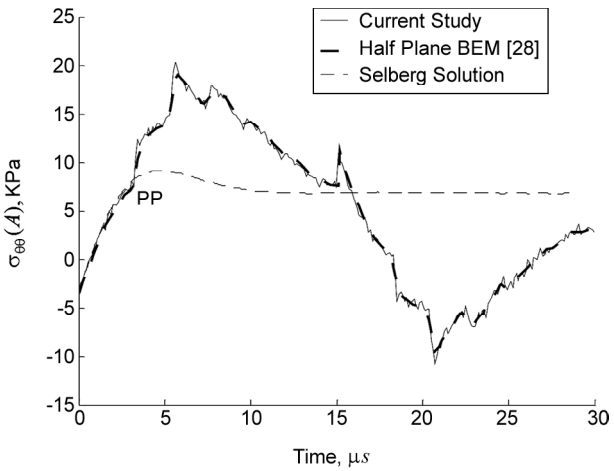

Figure 10. Comparison of hoop stress of point A with Green function BEM.

of the cavity and after reflection from the free surface arrives at point A. As shown in this figure, after this time, the response deviates from Selberg solution. The results for different values of Poisson's ratio are also shown in Figure 11. As shown in this figure, the Poisson's ratio which varies in a narrow range can significantly influence the results.

As shown in Figure (11), great amount of noise are observed for Poisson's ratio of 0.2, which is due to the element length and time interval values. The controlling parameter is β that is defined as:

$$\beta = \frac{C_S Dt}{l} \tag{14}$$

where l is the element length, Dt is the time interval equal to π / ω_{max}, and ω_{max} is the maximum circular frequency in the analysis. The values of β

for boundary elements in the surface of the cavity and the traction-free surface are shown in Table (1). There is a limiting value for β beyond which great amount of noise introduces into the numerical results. For wave propagation problem governed by scalar wave equation, the limiting value for β is suggested to be 0.6 [29].

From the above table, it can be concluded that the lower values for Poisson's ratio result in greater values of β and consequently more noise in the results.

For Poisson's ratio of $\frac{1}{3}$, a parametric study has been performed for different depths of the cavity. The results are depicted in Figure (12). As expected, by increasing the depth of the cavity, the time at which the response deviates from the Selberg solution increases and correspondingly the maximum value of the hoop stress decreases. In other words, for the large amount of depth, the hoop stress diagram experiences less fluctuations and converges to Selberg solution.

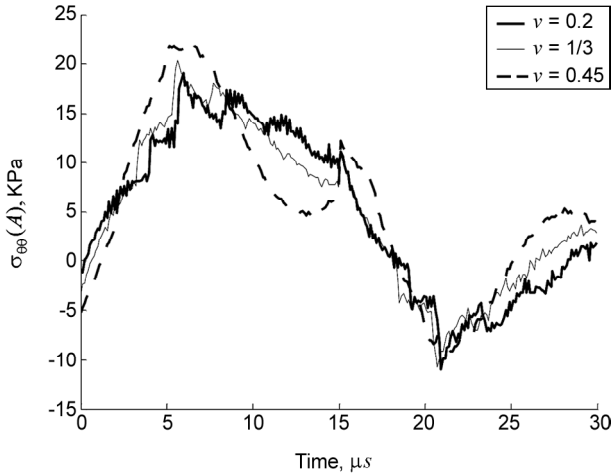

Figure 11. Hoop stress of point A for different values of Poisson's ratio.

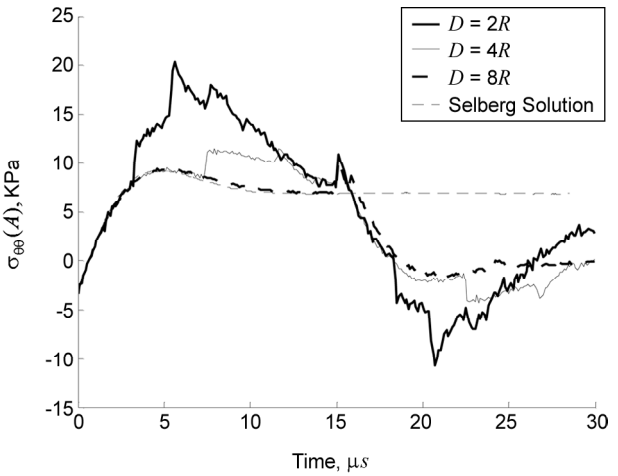

Figure 12. Hoop stress of point A for different depths of the cavity.

Table 1. Values of β for different boundaries of the model.

β	υ = 0.2	$\upsilon = \frac{1}{3}$	υ = 0.45
Surface Boundary	0.277	0.263	0.252
Cavity Boundary	0.564	0.535	0.513

5. Conclusion

In this study, the underground structure was simplified to cylindrical inclusion-half space model. The dynamic behavior of this model which involves uniform rectangular impulse pressure on the surface of the cavity was investigated by time-frequency domain BEM. Due to the dimension and impulsive loading condition of the problem, which may simulate the explosion in the cavity, very high frequencies have to be considered in the analysis. The stress of the boundary points are easily obtained from displacements and tractions at the cavity boundary without solving additional boundary integral equation. Some fluctuations are observed in time history of the hoop stress at the side point of the under-surface cavity, which represent the generation of different types of waves and multiple scattering of the waves between the cavity and the free surface boundaries.

For Selberg problem, it was shown that enclosing boundary of any arbitrary shape can be utilized successfully to model the infinitely extending boundaries. For this problem, the normalized radial displacement and the normalized hoop stress at the boundary of the cavity can be presented versus dimensionless time. It was also shown that the responses depend on the Poisson's ratio of the surrounding medium. For the case of inclusion-half space model, the response is also dependent on Poisson's ratio. Moreover, the depth of the cavity is another parameter that can influence the hoop stress of the cavity. It was shown that by increasing the depth of the cavity, the observed maximum value of the hoop stress decreases, and the hoop stress diagram converges to the Selberg solution.

References

1. Baron, M.L. and Matthews, A.T. (1961) Diffraction of a pressure wave by a cylindrical cavity in an elastic medium. *Journal of Applied Mechanics, Trans. ASME*, **28**, 345-354.

2. Lee, V.W. and Trifunac, M.D. (1979) Response of tunnels to incident SH waves. *Journal of Engineering Mechanics, Div.* ASCE, **105**, 643-659.

3. Tsaur, D. and Chang, K. (2012) Multiple scattering of SH waves by an embedded truncated circular cavity. *Journal of Marine Science and Technology*, **20**(1), 73-81.

4. Wong, K.C., Shah, A.H., and Datta, S.K. (1985) Dynamic stresses and displacements in a buried tunnels. *Journal of Engineering Mechanics*, ASCE, **111**, 218-234.

5. Valliappan, S., Chandrasekaran, V., and Lee, I.K. (1979) Interaction between tunnel openings due to vibration effects. Wittke, W. (Ed.), *Numerical Methods in Geomechanics*, 685-697, Balkema, Rotterdam.

6. Manolis, G.D. and Beskos, D.E. (1982) Dynamic response of framed underground structures. *Computers and Structures*, **15**, 521-531.

7. Alheid, H.J., Hinzen, K.G., Honecker, A., and Safeld, W. (1988) Response of underground openings to earthquakes and blast loading. Swoboda, G. (Ed.), *Numerical Methods in Geomechanics, Balkema, Rotterdam*, 1689-1696.

8. Ang, A.H.S. and Newmark, N.M. (1963) *Computation of Underground Structural Response*. DASA Report, No. 1386, University of Illinois, Urbana.

9. Benites, R., Aki, K., and Yomogida, K. (1992) Multiple scattering of SH waves in 2-D media with many cavities. *Pure Applied Geophysics*, **138**(3), 353-390.

10. Luco, J.E. and de Barros, F.C.P. (1994) Dynamic displacements and stresses in the vicinity of a cylindrical cavity embedded in a half-space. *Earthquake Engineering and Structural Dynamics*, **23**(3), 321-340.

11. Alielahi, H., Kamalian, M., Asgari Marnani, J., Jafari, M.K., and Panji, M. (2013) Applying a time-domain boundary element method for study of seismic ground response in the vicinity of embedded cylindrical cavity. *International Journal of Civil Engineering*, Transaction B: Geotechnical Engineering, **11**(1), 45-54.

12. Panji1, M., Kamalian, M., Asgari Marnani, J., and Jafari, M.K. (2013) Transient analysis of wave propagation problems by half-plane BEM. *Geophysical Journal International*, **194**(3), 1849-1865.

13. Kobayashi, S. and Nishimura, N. (1982) Transient stress analysis of tunnels and caverns of arbitrary shape due to travelling waves. Banerjee, P.K., Shaw, R.P. (Eds.), *Developments in Boundary Element Methods*, Elsevier Applied Science, London, 177-210.

14. Kontoni, D.P.N., Beskos, D.E., and Manolis, G.D. (1987) Uniform halfplane elastodynamic problems by an approximate BEM. *Earthquake Engineering and Structural Dynamics*, **6**, 227-238.

15. Yu, C.W. and Dravinski, M. (2009) Scattering of plane harmonic P, SV and rayleigh waves by a completely embedded corrugated cavity. *Geophysical Journal International*, **178**, 479-487.

16. Shah, A.H., Wong, K.C., and Datta, S.K. (1982) Diffraction of plane SH waves in a half-space. *Earthquake Engineering and Structural Dynamics*, **10**, 519-528.

17. Benites, R., Aki, K., and Yomogida, K. (1992) Multiple scattering of SH waves in 2-D media with many cavities, *Pure and Applied Geophysics*, **138**(3), 353-390.

18. Panji, M., Kamalian, M., Asgari Marnani, J., and Jafari, M.K. (2014) Antiplane seismic response from semi-sine shaped valley above embedded truncated circular cavity: a time-domain half-plane BEM. *International Journal of Civil Engineering, Transaction B: Geotechnical Engineering*, **12**(2), 193-206.

19. Dravinski, M. (1983) Ground Motion Amplifica-

tion due to Elastic Inclusions in a Half-space. *Journal of Earthquake Engineering and Structural Dynamics*, **11**, 313-335.

20. Rajapakse, R.K.N.D. and Senjuntichai, T. (2000) 'Steady-state dynamic response of poroelastic media'. In: *Wave Motion in Earthquake Engineering*, Kausel, E., Manolis, G. (Eds.), Chapter 8, WIT press, Southampton and Boston, 283-313.

21. Dominguez, J. (1993) *Boundary Elements in Dynamics*. Computational Mechanics Publications, Southampton and Boston.

22. Ameen, M. (2001) *Boundary Element Analysis; Theory and Programming*. Alpha Science International, UK.

23. Ahmad, S. and Banerjee, P.K. (1988) Multi-domain BEM for two-dimensional problems of elastodynamics. *International Journal for Numerical Methods in Engineering*, **26**(4) 891-911.

24. Heymsfield, E. (1997) Infinite domain correction for anti-plane shear waves in a two-dimensional boundary element analysis. *International J. for Numerical Methods in Engineering*, **40**(5), 953-964.

25. Kamalian, M., Gatmiri, B., and Sohrabi, A. (2003) On time-domain two-dimensional site response analysis of topographic structures by BEM. *Journal of Seismology and Earthquake Engineering (JSEE)*, **5**(2), 35-45.

26. Shen, S-Y. (2003) An indirect elastodynamic boundary element method with analytic bases. *International Journal for Numerical Methods in Engineering*, **57**, 767-794.

27. Frangi, A. (1999) Elastodynamics by BEM: A new direct formulation. *International Journal for Numerical Methods in Engineering*, **45**, 721-740.

28. Richter, C. and Schmid, G. (1999) A Green's function time-domain boundary element method for the elastodynamic half-plane. *International Journal for Numerical Methods in Engineering*, **46**, 627-648.

29. Mansur, W.J. (1983) *A Time-Stepping Technique to Solve Wave Propagation Problems using the Boundary Element Method*. Ph.D. Thesis, University of Southampton, England.